*J. Fluid Mech.* (1995), *vol.* 301, *pp.* 37–50



# Reconsideration of oblique shock wave reflections in steady flows. Part 2. Numerical investigation

By J. VUILLON[1], D. ZEITOUN[1] AND G. BEN-DOR[2]

[1] Systemes Energetiques et Transferts Thermiques, Universite de Provence, Marseille, France

[2] Pearlstone Center for Aeronautical Engineering Studies, Department of Mechanical Engineering, Ben-Gurion University of the Negev, Beer Sheva, Israel

(Received 20 May 1994 and in revised form 18 May 1995)

The reflection of shock waves over straight reflecting surfaces in steady flows was investigated numerically with the aid of the LCPFCT algorithm. The findings completely supported the experimental results which were reported in Part 1 of this paper (Chpoun *et al.* 1995). In addition, the dependence of the resulting shock wave configuration on the distance between the trailing edge of the reflecting wedge and the bottom surface, inside the dual-solution domain, was studied. As a result of this study, as well as the one reported in Part 1, the state of the art of shock wave reflections in steady flows was reconsidered.

## 1. Introduction

A detailed discussion of the two shock wave reflection configurations which are possible in steady flows, i.e. regular (RR) and Mach (MR) reflections, and the various possible transition criteria between them, are given in part 1 of the present study (Chpoun *et al.* 1995).

In addition, the state of the art as it existed when our experimental (Part 1) and numerical (present) studies began are also summarized in Chpoun *et al.* (1995).

### *The* RR↔MR *transition*

Following Li's (1995) conclusions, an experimental study of the RR↔MR transition in steady flows was conducted by Chpoun *et al.* (1985) in the supersonic wind tunnel of Laboratoire d'Aerothermique du CNRS, Meudon, France. Their experimental results verified Li's (1995) conclusions. Both the analytical and experimental results indicated that there are regions in the dual-solution domain in which the regular reflection wave configuration is stable and that the RR→MR transition could occur anywhere in that domain, i.e. $\omega_i^N \leqslant \omega_i^{tr}(\mathrm{RR}\rightarrow\mathrm{MR}) \leqslant \omega_i^D$.

Chpoun *et al.* (1995) also concluded that the wave configuration that is actually established in the dual-solution domain probably depends on geometrical parameters which arise from both the experimental facility used and the specific experimental set-up. The exact way by which the above-mentioned geometrical parameters affect the phenomenon is not yet clear. Some ideas can be found in Hornung, Oertel & Sandeman's (1979) study of the RR↔MR transition process in which the 'lengthscale' concept was put forward. This dependence on geometrical parameters, however, could explain why Hornung & Robinson (1982) and Henderson & Lozzi (1975, 1979) failed to observe stable RR wave configurations inside the dual-solution domain, while Chpoun *et al.* (1995) did observe stable RR wave configurations there.

Since recent analytical (Li 1995) and experimental (Chpoun *et al.* 1995) studies indicated that, depending on geometrical conditions, both RR and MR wave configurations are stable in the dual-solution domain, it was decided to numerically investigate the reflection phenomenon in steady flows in order to shed more light on and deepen our understanding of how the geometrical parameters affect the reflection process inside the dual-solution domain.

As will be shown subsequently, the numerical simulations revealed that both RR and MR are indeed stable in the dual-solution domain and that the specific type of reflection, i.e. RR or MR, indeed depends on the geometrical set-up of the numerical experiment.

Prior to our introducing the present numerical study and results, it should be noted that Auld & Bird (1976) had already investigated this phenomenon. Their calculations were carried out at the molecular level using a direct simulation Monte Carlo method. Their numerical results 'strongly indicated that regular reflection can occur in the range of deflection angles for which both regular and Mach reflection are possible'. Note that at the time of their study regular reflection wave configurations were considered to be unstable in that domain.

## 2. The numerical study

Details of the numerical study are given in the following. First, the governing equations of the problem under investigation are presented. Then, the numerical method for solving the governing equations, as well as additional data relevant to the numerical solution, are outlined. Finally, the geometrical set-up of the numerical simulation is discussed. Many more details regarding the numerical investigation can be found in Vuillon (1994).

### 2.1. *The governing equations*

The two-dimensional unsteady Euler equations which describe a non-dissipative flow over a wedge in Cartesian $(x, y)$ geometry are

$$\frac{\partial \rho}{\partial t} = -\frac{\partial}{\partial y}(\rho v) - \frac{\partial}{\partial x}(\rho u), \tag{1a}$$

$$\frac{\partial (\rho u)}{\partial t} = -\frac{\partial}{\partial y}(\rho uv) - \frac{\partial}{\partial x}(\rho uu) - \frac{\partial P}{\partial x}, \tag{1b}$$

$$\frac{\partial (\rho v)}{\partial t} = -\frac{\partial}{\partial y}(\rho vv) - \frac{\partial}{\partial x}(\rho vu) - \frac{\partial P}{\partial y}, \tag{1c}$$

$$\frac{\partial (\rho E)}{\partial t} = -\frac{\partial}{\partial y}[(E+P)v] - \frac{\partial}{\partial x}[(E+P)u], \tag{1d}$$

where $u$ and $v$ are the flow velocity components in the respective $x$- and $y$-directions, $P$ and $\rho$ are the local pressure and density and $E$ is the total energy per unit mass. To close the system, the pressure and the total energy are related by

$$E = \frac{P}{\gamma - 1} + \tfrac{1}{2}\rho(u^2 + v^2), \tag{2}$$

where $\gamma$ is the specific heat capacities ratio. The right-hand sides of the above equations are separated into two parts, the $y$-direction terms and the $x$-direction terms. This

arrangement in each of the four equations separates the $y$-derivatives and the $x$-derivatives in the divergence and gradient terms into parts which can be treated sequentially by a general one-dimensional solver.

To use this split-step approach, one must ensure that the time step chosen is small enough to ensure that the distinct components of the fluxes do not change the cell average values appreciably during the time step.

### 2.2. *The numerical method*

The method used for the presented numerical simulation is the LCPFCT algorithm of Boris *et al.* (1993) which is a Flux-Corrected Transport (FCT) algorithm for solving generalized continuity equations. This algorithm is one of the latest one-dimensional flux corrected transport (FCT) algorithms with fourth-order phase accuracy and minimum residual diffusion. Moreover, one-dimensional continuity equation solvers such as LCPFCT can be used repetitively to construct a multi-dimensional program by time-step splitting in the different coordinate directions. The split method implemented here has been described previously and is very convenient in the present case.

The boundary conditions on the different sides of the integration domain were as follows (see figure 1): supersonic inflow conditions are imposed upstream; a relaxation to infinity values was implemented on both the downstream and the upper sides; the lower side was an axis of symmetry which in the case of an Eulerian approach was equivalent to a perfect wall; wall conditions were selected everywhere around the wedge.

The reliability of the computer code developed was checked by simulating Hornung & Robinson's (1982) experimental results. A comparison between the Mach stem height as predicted by the numerical simulation (open circles) and Hornung & Robinson's (1982) measurements (closed circles) for the flow Mach numbers $M_0 = 2.84$ and 3.98 is shown in figure 2. The solid lines are the predictions of Azevedo's (1989) analytical model. Figure 2 clearly indicates that the numerical simulation is capable of excellently reproducing the experimental results.

In addition to this comparison, the angles between the various discontinuities of the triple point were compared to those obtained analytically and/or experimentally by Chpoun *et al.* (1995). The agreement was again excellent. Based on these comparisons, it was concluded that the numerical code, which was developed in the course of this study, was capable of accurately simulating the investigated phenomenon.

*Grid and time-step considerations*

To implement the geometry of the problem, the Cartesian grid was chosen by fitting the wedge angle with the spatial steps in each direction ($\Delta x = \Delta y/\tan\theta_w$). Then sequential integration in each of the coordinate directions was performed without taking into account the internal points of the wedge. The result was that various geometries of the wedge could be studied by using only Cartesian grids.

The LCPFCT algorithm is an explicit finite difference scheme and its time step is submitted to the CFL stability criterion. This criterion, for a given integration direction, depends on the flow field fluctuation in this particular direction and is expressed by

$$\Delta t = \min \sum_i \frac{\Delta L_i}{v_i + a_i}, \tag{3}$$

where $\Delta L_i$ is the spatial step, $v_i$ and $a_i$ are the respective velocity and sound speed of

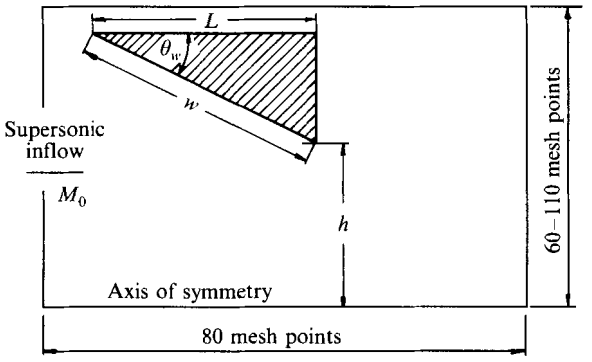


FIGURE 1. Schematic illustration of the numerical set-up. $M_0$, incident flow Mach number; $\theta_w$, reflecting wedge angle; $w$, length of the reflecting wedge surface; $h$, exit cross-sectional area; $L$, length of the reflecting wedge.

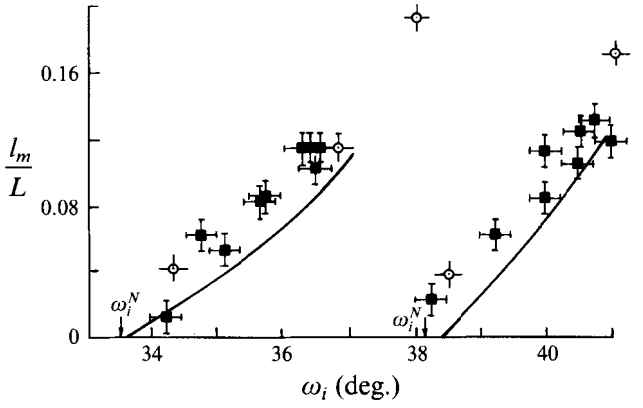


FIGURE 2. Comparison between the Mach stem height as predicted by the numerical code developed here (open circles) and as observed experimentally by Hornung & Robinson (1982) (closed circles). For $M_0 = 2.84$ and 3.98 the error bars are indicated for each point. The solid lines were calculated by Azevedo (1989). $h/L = 0.37$.

the integration direction considered. Recall that $v_i$ is actually $u$ in the $x$-direction and $v$ in the $y$-direction, as given in equations (1) and (2).

The grid spacing in the $y$-direction (vertical) was set to be constant and equal to $\Delta y = 1$ mm. In the $x$-direction (horizontal) the grid spacing was deduced for a given wedge having an angle of $\theta_w$ from the relation $\Delta x = \Delta y/\tan\theta_w$. The computational domain was meshed by 80 points in the $x$-direction and by between 60 and 110 points in the $y$-direction, depending on the value of the exit cross-sectional area, $h$ (see figure 1).

At $t = 0$ the flow quantities were initialized with the upstream flow conditions. The integration time step depended on the flow fluctuations and had an average value of 0.6 μs. The steady-state Mach reflection wave configurations were obtained after about 3000 iterations when the $L_2$-norm residual had dropped by more than five orders of magnitude. The CPU time was about $8.3 \times 10^{-5}$ s/pt/iter. on an IBM 3090-VF computer.

Consequently, the above-mentioned mesh sizes were chosen in order to get a steady solution in a reasonable CPU time. However, it had been verified, particularly through the wave angles at the triple point and the location of the Mach stem, that the solutions

obtained were identical to those obtained with a finer grid (for more details see Vuillon 1994).

### 2.3. *The geometrical set-up*

The geometrical and numerical set-up in the present numerical simulation is shown schematically in figure 1. The oncoming flow Mach number is $M_0$, the reflecting wedge angle is $\theta_w$, the distance between the leading and trailing edges of the reflecting wedge is $w$ and the distance from the trailing edge of the reflecting wedge to the line of symmetry is $h$. (Note that since the problem under consideration is two-dimensional, $h$ could be regarded as the exit cross-sectional area.)

Based on theoretical considerations the distance $h$ is bounded by lower and upper limits. The lower limit on $h$, i.e. $h_{min}$, corresponds to the case in which the reflected shock wave, r of a stable Mach reflection, grazes the trailing edge of the reflecting wedge. This limiting situation is shown in figure 3(*a*). Whenever the distance $h$ reaches this value or is reduced below it, i.e. $h \leqslant h_{min}$, the Mach reflection becomes unstable and its Mach stem moves upstream until the Mach reflection vanishes and a bow shock wave is established ahead of the leading edge of the reflecting wedge. As a result, the flow through the two-dimensional converging nozzle, formed by the surface of the reflecting wedge and the line of symmetry, becomes subsonic. The two-dimensional converging nozzle which is formed by the wedge and bottom surfaces is said to be *unstarted* for this case.

The value of $h_{min}$ can be calculated using geometrical relations from

$$h_{min} = w\left[\frac{\sin\phi_1 \sin\phi_2}{\sin(\phi_1+\phi_2-\theta_w)} - \sin\theta_w\right] + l_m, \tag{4}$$

where $\phi_1$ and $\phi_2$ are the angles of incidence of the incident and reflected shock waves, respectively, $w$ is the length of the reflecting surface, and $l_m$ is the height of the Mach stem. The angle of incidence $\phi_1$ can be simply obtained from

$$\tan\theta_w = \frac{(M_0^2\sin^2\phi_1 - 1)\cot\phi_1}{\frac{1}{2}(\gamma+1)M_0^2 - (M_0^2\sin^2\phi_1 - 1)}. \tag{5}$$

The angle of incidence $\phi_2$ can be obtained by solving the governing equations of the Mach reflection, i.e. the three-shock theory (for details see Ben-Dor 1991, p. 13), and the Mach stem height, $l_m$, can be obtained using Azevedo's (1989) model (see also Azevedo & Liu 1993).

The upper limit on $h$, i.e. $h_{max}$, is determined by the point where the leading characteristic of the expansion fan, which is formed at the trailing edge of the reflecting wedge, intersects the incident shock wave, as shown in figure 3(*b*). Using geometrical relations it can be simply shown that

$$h_{max} = w\frac{\sin\theta_w \sin(\theta_w+\mu_1)}{[\sin\mu_1 \sin\phi_1/\sin(\phi_1-\theta_w)] - \sin(\theta_w+\mu_1)}, \tag{6}$$

where the angle of incidence, $\phi_1$, can be calculated from equation (5). The Mach angle, $\mu_1$, is simply obtained from

$$\mu_1 = \sin^{-1}(1/M_1), \tag{7}$$

where the flow Mach number, $M_1$, behind the incident shock wave is given by

$$M_1^2 = \frac{M_0^2\sin^2\phi_1 + (2/\gamma - 1)}{((2\gamma/\gamma - 1)M_0^2\sin^2\phi_1 - 1)\sin^2(\phi_1-\theta_w)}. \tag{8}$$

In (5) and (8) $\gamma$ is the ratio of the specific heat capacities, i.e. $\gamma = C_p/C_v$.

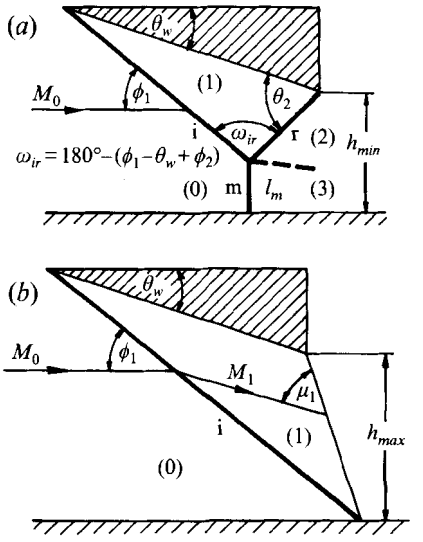


FIGURE 3. Schematic illustration of the lower (*a*) and upper (*b*) limits on the exit cross-sectional area, $h$, i.e. $h_{min}$ and $h_{max}$, respectively: i, incident wave; r, reflected wave; m, Mach stem shock waves; $\omega_{ir}$, angle between i and r; $l_m$, Mach stem length; $\phi$, angles of incidence; $\mu$, Mach angle.

Based on the foregoing discussion, it can be concluded that for a given combination of flow Mach number, $M_0$, reflecting wedge angle, $\theta_w$, and reflecting wedge length, $w$, a reflection, either RR or MR, will occur provided the exit cross-sectional area at the trailing edge, $h$, is in the interval

$$h_{min} < h < h_{max}.$$

Prior to presenting our numerical results in the interval $h_{min} < h < h_{max}$, it is of interest to illustrate the transient process which takes place when $h \leqslant h_{min}$, i.e. a case, which as mentioned earlier, corresponds to a situation in which the two-dimensional converging nozzle formed by the reflecting wedge and the line of symmetry is said to be unstarted.

The various colours in figures 4 and 6 correspond to various densities as shown in the colour scale given in figure 4(*a*). The reflecting wedge is shown in these figures in red.

## 3. Results

### 3.1. *The wave evolution for* $h \leqslant h_{min}$

The transient process which takes place for $M_0 = 2.84$, $\theta_w = 26.56°$, $w = 7$ cm and $h = 3.9$ cm is shown in figures 4(*b–f*). Since $h_{min}$ for these conditions as obtained from equation (4) is about 4 cm, this is clearly a case for which $h < h_{min}$.

Figure 4(*b*) shows a non-stationary Mach reflection. The Mach stem propagates upstream as shown in the successive computational results in figure 4(*c*) where the reflected shock wave of the Mach reflection is seen to hit the trailing edge of the reflecting wedge. As a result, see figure 4(*d*), the reflected shock wave of the non-stationary Mach reflection reflects over the surface of the reflecting wedge as a secondary Mach reflection. Figure 4(*e*) shows the wave configuration shortly before

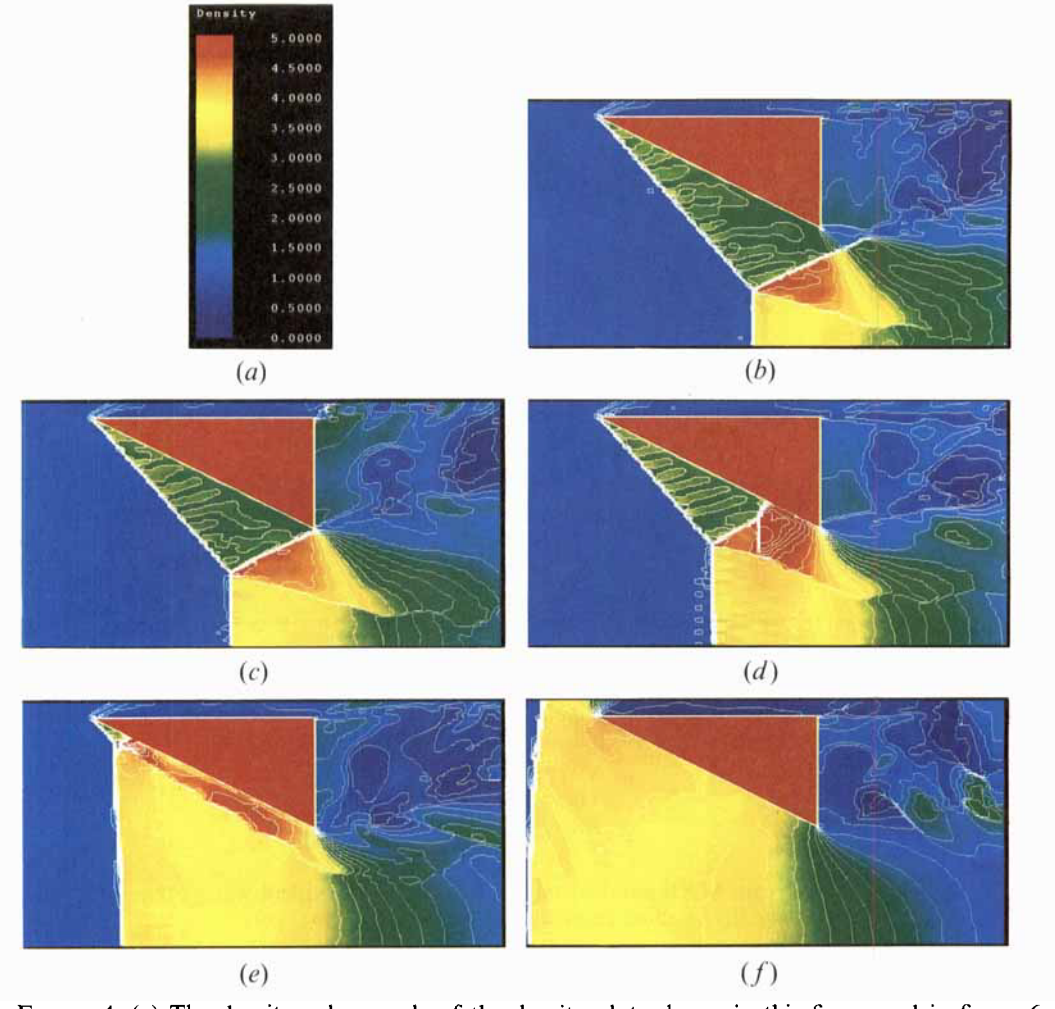


FIGURE 4. (*a*) The density colour scale of the density plots shown in this figure and in figure 6. Numerical simulations (density contours) appropriate to the case $h < h_{min}$ in which the process finally results in a bow shock wave ahead of the reflecting wedge. $M_0 = 2.84$ and $\theta_w = 26.56°$. (*b*, *e*) Non-stationary MR wave configurations in which the Mach stem propagates upstream. Note how the reflected shock wave reflects over the surface of the reflecting wedge as a Mach reflection. (*f*) A stationary bow shock wave ahead of the reflecting wedge. The two-dimensional converging nozzle is unstarted for this case.

the Mach stem of the secondary Mach reflection reaches the leading edge of the reflecting wedge. The stable bow shock wave which is finally established ahead of the unstarted two-dimensional converging nozzle is shown in figure 4(*f*). Unlike the non-stationary Mach reflection shown in figures 4(*b–e*), the bow shock wave shown in figure 4(*f*) is stationary. The subsonic flow behind it accelerates as it passes through the two-dimensional converging nozzle.

### 3.2. *The reflection configurations for* $h_{min} < h < h_{max}$

Seven different cases were investigated numerically in this region. The upstream Mach number, $M_0$, and the reflecting wedge angle, $\theta_w$, are given in table 1. In addition, as indicated in figure 5, where the position of the seven cases in the $(M_0, \omega_i)$-plane is

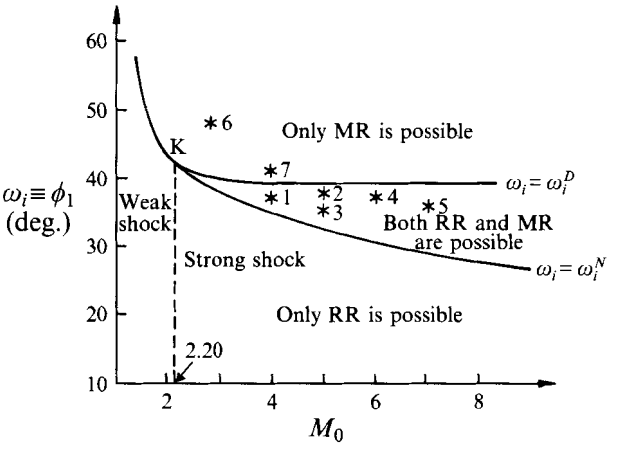


FIGURE 5. Domains of different types of reflections in the $(M_0, \omega_i)$-plane for $\gamma = 1.4$. $\omega_i^D$ is the detachment condition, and $\omega_i^N$ the von Neumann condition. Numbered stars show the cases listed in table 1.

| Case | $M_0$ | $\theta_w$ | $\phi_1 = \omega_i$ |
|---|---|---|---|
| 1 | 3.98 | 23.6° | 36.8° |
| 2 | 4.96 | 26.56° | 37.8° |
| 3 | 4.96 | 25.0° | 35.5° |
| 4 | 6.00 | 26.56° | 37.0° |
| 5 | 7.00 | 26.56° | 35.5° |
| 6 | 2.84 | 26.56° | 48.0° |
| 7 | 3.98 | 26.56° | 41.25° |

TABLE 1. Upstream Mach number, reflecting wedge and incident wave angles of the investigated cases. For all the wedges $w = 7$ cm.

shown, cases 1–5 are located inside the dual-solution domain in which both RR and MR are theoretically possible and cases 6 and 7 are located in the domain in which only MR is possible.

A few simulations with increasing values of $h$ were conducted for each of these cases. Typical simulations for case 2 for which $M_0 = 4.96$ and $\theta_w = 26.56°$ are shown in figures 6(*a–d*). In figure 6(*a*), in which $h$ is slightly larger than $h_{min}$, a clear Mach reflection is observed. When $h$ is increased, the triple point moves backwards (downstream) and the height of the Mach stem decreases (see figures 6*b* and 6*c*). Further increase of $h$ finally results in a situation in which the Mach stem vanishes and the reflection becomes regular. Such a situation is shown in figure 6(*d*) where a clear regular reflection is seen. Based on the numerical simulations the MR $\leftrightarrow$ RR transition occurred for this case at $h_{tr} = 5.65$ cm. Note that for the conditions of case 2 equation (6) results in $h_{max} = 5.9$ cm.

A similar procedure was employed to numerically investigate cases 1, 3, 4 and 5 (see table 1) which, as shown in figure 5, also lie inside the dual-solution domain. The numerically determined values of $h$ at which the MR $\leftrightarrow$ RR transition occurred, i.e. $h_{tr}$, as well as the values of $h_{max}$ as calculated for each of these cases from equation (6) are given in table 2.

As can be seen from table 2, $h_{tr}$ is smaller than $h_{max}$. This is also shown in figure 7

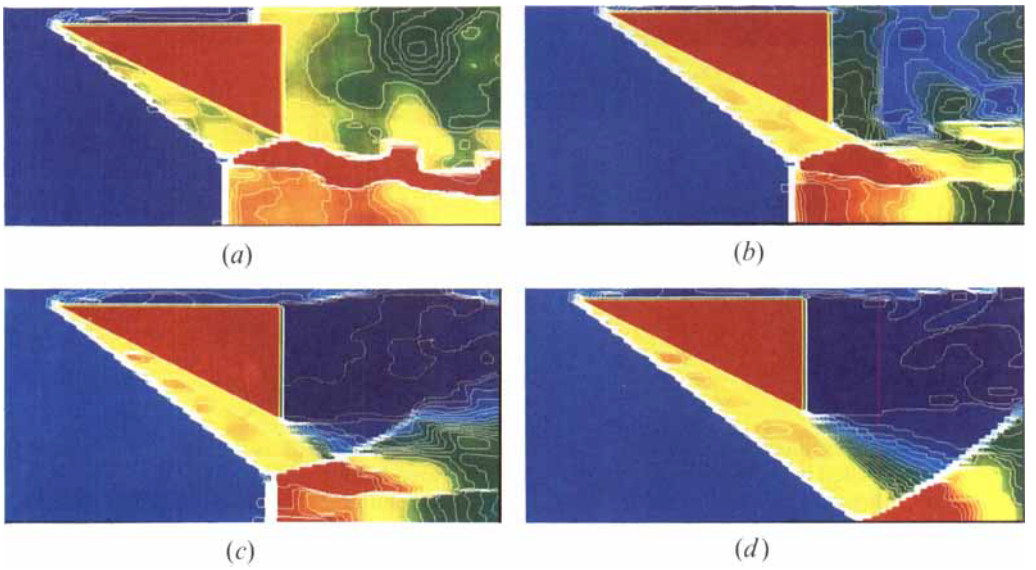


FIGURE 6. Numerical simulations (density contours) appropriate to the case $h_{min} < h < h_{max}$ in which the MR↔RR transition is shown to occur $M_0 = 4.96$ and $\theta_w = 26.56°$. (*a–c*) Successive stationary Mach reflections with increasing values of $h$. Note how the Mach stem which moves downstream becomes shorter. (*d*) A stationary regular reflection. The colour scale of the density plots is shown in figure 4(*a*).

| Case | $h_{tr}$ (cm) | $h_{max}$ (cm) |
|---|---|---|
| 1 | 5.85 | 7.85 |
| 2 | 5.65 | 5.90 |
| 3 | 5.05 | 5.70 |
| 4 | 4.85 | 5.15 |
| 5 | 4.65 | 5.10 |

TABLE 2. The numerically determined values of $h_{tr}$ where the MR↔RR transition takes place. $M_0$, $\theta_w$ and $w$ are given in table 1.

in which the seven simulations which have been conducted in case 1 of table 1 are superimposed. The solid line is the incident shock wave, the dashed–dotted line is the locus of the feet of the Mach stems of the Mach reflection wave configurations (for clarity the reflected shock waves and the slipstreams of the Mach reflection wave configurations are not drawn in figure 7). The point where the dashed–dotted line intersects the incident shock wave is the point where the RR↔MR transition occurs. Although the dashed–dotted line seems to be straight, it is not. The numerical simulations clearly indicated that it is curved near the point where the RR↔MR transition is obtained. The dashed line in figure 7 is the head of the expansion fan which is formed at the trailing edge of the reflecting wedge. The point where the head of the expansion fan intersects the incident shock wave determines the value of $h_{max}$. For values of $h > h_{max}$ the original incident shock wave ceases to exist since its strength decreases as a result of its continuous interaction with the entire expansion fan.

Combining the information given in tables 1 and 2 indicates that $h_{tr}$ decreases as the incident flow Mach number increases, which is also shown in figure 8 in the $(M_0, h)$-

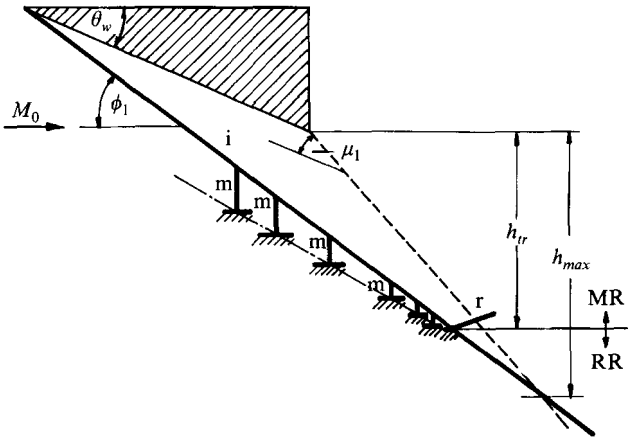


FIGURE 7. Schematic illustration of the decrease in the Mach stem height as the transition from MR to RR is approached by increasing the exit cross-sectional area $h$, for the same initial gasdynamic ($M_0$ and $\phi_1$) conditions, $M_0 = 3.98$, $\theta_w = 23.6°$. The numerically resulting wave configurations are MR as long as $h < h_{tr}$, and RR when $h > h_{tr}$. Note that $h_{max} > h_{tr}$.

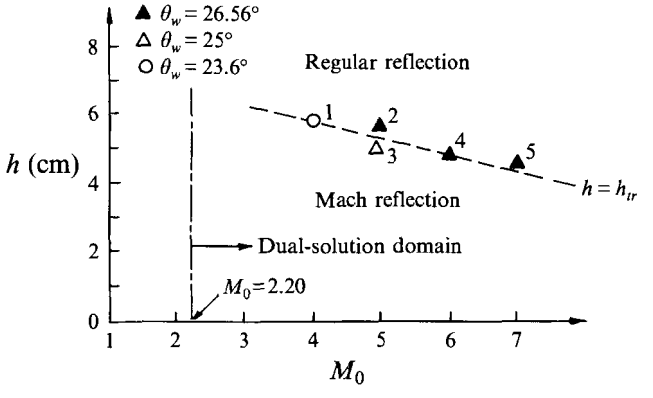


FIGURE 8. The dependence of $h_{tr}$ on $M_0$ inside the dual-solution domain as obtained numerically. Exact conditions for cases 1–5 are given in table 1.

plane. Note that for cases 2, 4 and 5, $\theta_w = 26.56°$ and hence these three simulations clearly indicate the dependence of $h_{tr}$ on $M_0$ for a fixed $\theta_w$. For the other two cases, 1 and 3, $\theta_w$ is somewhat smaller.

From cases 3 and 5 for which $\omega_i$ is practically the same (see table 1), a slight dependence of $h_{tr}$ on $M_0$ for a fixed $\omega_i$ is evident. When the above-mentioned numerical investigation procedure was conducted for cases 6 and 7 (see table 1) which, as shown in figure 5, lie in the domain in which only Mach reflection is theoretically possible, the reflection was still a Mach reflection when $h$ reached the value of $h_{max}$, as shown for case 6 in figure 9. (Note that unlike figure 7, here the reflected shock waves are also drawn.). It is evident from figure 9 that if the loci of the feet of the Mach stems of the Mach reflection wave configurations are extrapolated to intersect the incident shock wave, the intersection point is at a value $h > h_{max}$. However, since as mentioned earlier, at $h > h_{max}$ the incident shock wave undergoes a continuous decrease in its strength owing to its continuous interaction with the expansion fan, which emanates from the trailing edge of the reflecting wedge, it can no longer be regarded as the original

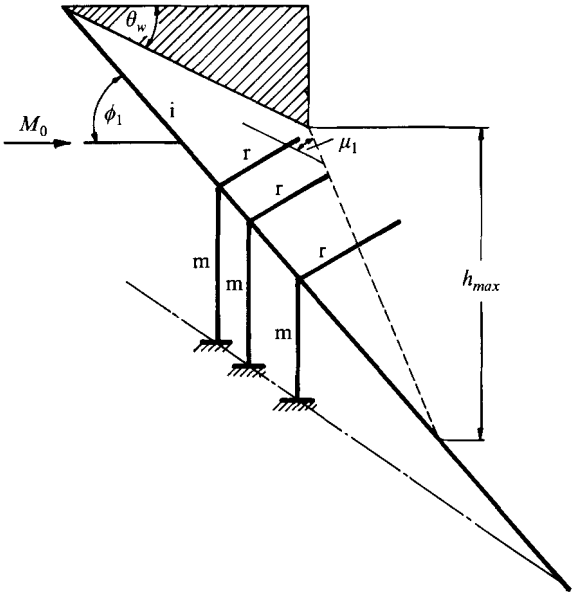


FIGURE 9. Schematic illustration of the decrease in the Mach stem height as the exit cross-sectional area, $h$, is increased, for $M_0 = 2.84$, $\theta_w = 26.56°$. Note that when $h$ reaches $h_{max}$ the numerically resulting wave configuration is still an MR. A transition to RR would have occurred near the point where the incident show wave is intersected by the locus of the feet of the Mach stems of the Mach reflections (dashed–dotted line) which is far below $h_{max}$; however, at that location the incident shock wave is already weakened as a result of its continuous interaction with the expansion fan which is formed at the trailing edge of the reflecting wedge.

incident shock wave. Thus, it is not surprising that for cases similar to 6 and 7 (see figure 5) which lie in the domain in which only Mach reflection is possible, $h = h_{max}$ is reached when the reflection is still Mach reflection and a transition to regular reflection is impossible.

### 3.3. *Stability of the regular reflection wave configuration*

The stability of the regular reflection wave configuration, which was established inside the dual-solution domain, was investigated by numerically introducing a pressure disturbance behind its reflection point. This was carried out in the following way. When a stationary regular reflection was established in the dual-solution domain, it was disturbed by introducing an overpressure and forcing the flow velocity to be equal to zero in the computational domain extending downstream of the reflection point for a height of 5 grid points. This way of introducing the overpressure disturbance was found to be sufficient to force the regular reflection to undergo a transition to become a Mach reflection. Following the formation of the Mach reflection the code was kept running for a wide number of iterations until the solution again became stationary. Using this procedure of introducing a disturbance it was found that:

(i) regular reflection wave configurations which were formed in the range $h_{min} < h < h_{tr}$ were not stable and the finally observed reflection in this range was always a Mach reflection;

(ii) regular reflection wave configurations which were formed in the range $h_{tr} < h < h_{max}$ were stable. The Mach reflection which was formed following the introduction of the disturbance eventually vanished and the finally observed stable reflection in this range was again regular reflection.

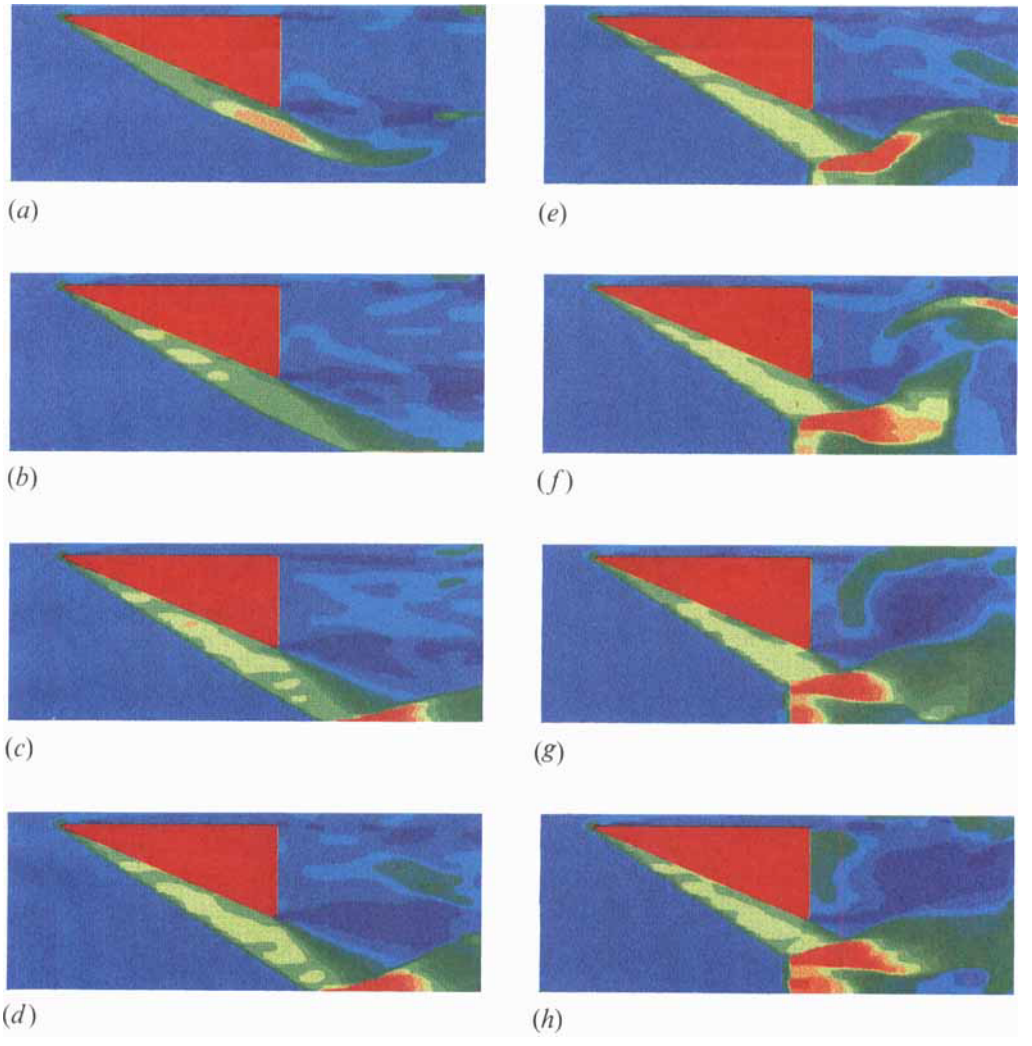


FIGURE 10. Illustration of the numerical evolution of the flow prior to and after the introduction of an overpressure disturbance in the dual-solution domain. Soon after the supersonic flow interacts with the reflecting wedge, the incident shock wave is formed (*a*). The incident shock wave, which is not yet straight, encounters the line of symmetry and the reflected shock wave is generated (*b*). A regular reflection is finally generated by the numerical code (*c*). A pressure disturbance is introduced behind the reflection point (*d*). The disturbance forces the RR to undergo a transition to MR (*e*). The MR stabilizes (*f* and *g*) until it reaches its stationary configuration (*h*).

Figure 10 shows the above-described procedure of disturbance introduction for $M_0 = 4.96$, $\theta_w = 23°$ and $h_{min} < h < h_{tr}$. Following the initiation of the flow, the regular reflection shown in (*c*) was established. The above-mentioned pressure and velocity disturbances were introduced numerically in (*d*). As a result, the regular reflection vanished and a Mach reflection (shown in *e*) was formed. After the code completed a wide number of iterations, a stable Mach reflection wave configuration (*g* and *h*) was established.

## 4. Conclusions

A numerical investigation of steady shock wave reflections in the dual-solution domain in which, based on the two- and three-shock theories, both regular and Mach reflection wave configurations are theoretically possible, revealed that in contrast to the accepted state of the art which was established by Hornung & Robinson (1982), regular reflection wave configurations are stable in this domain. The numerical finding supports an analytical study of Li (1995) who showed recently that, based on the principle of minimum entropy production, regular reflection wave configurations should be stable in most of the dual-solution domains.

In addition, the numerical investigation illustrated how the resulting wave configuration depends on the geometrical set-up. It was shown that for the same initial gasdynamic conditions, i.e. incident flow Mach number, $M_0$, reflecting wedge angle, $\theta_w$ (i.e. angle of incidence $\phi_1$) and reflecting wedge surface length, $w$, the resulting stable wave configuration can be either a Mach or a regular reflection depending upon whether the exit cross-sectional area, $h$, is smaller or larger than a critical cross-sectional area, $h_{tr}$, at which the MR$\leftrightarrow$RR transition occurred. In the range $h_{min} < h < h_{tr}$ the stable wave configurations were Mach reflections and in the range $h_{tr} < h < h_{max}$ the stable wave configurations were regular reflections. Regular reflection wave configurations, which were established in the range $h_{min} < h < h_{tr}$ were found to be unstable. Small numerical disturbances forced them to vanish and give rise to Mach reflection wave configurations. Our numerical attempts to establish Mach reflection wave configurations in the range $h_{tr} < h < h_{max}$ failed. Unfortunately, because the reflection depends on many other geometrical parameters, we could not compare our findings quantitatively with experimental results. However, all the phenomena which were found to occur in our numerical simulations were observed experimentally by Chpoun *et al.* (1995).

Finally, it was shown that in the domain where theoretically only Mach reflection wave configurations are possible, the numerically established wave configurations were indeed Mach reflections in the entire range $h_{min} < h < h_{max}$.

## REFERENCES


ANDERSON, J. D. 1982 *Modern Compressible Flow.* McGraw-Hill.

AULD, D. J. & BIRD, G. A. 1976 The transition from regular to Mach reflection. *AIAA 9th Fluid and Plasma Dynamics Conf., San-Diego, California, July 14–16.* (See also *AIAA Paper* 76-322.)

AZEVEDO, D. J. 1989 Analytical prediction of shock patterns in a high-speed wedge bounded duct. PhD thesis, Dept. Mech. & Aero. Engng, State University of NY Buffalo.

AZEVEDO, D. J. & LIU, S. L. 1993 *AIAA J.* **31**, 83–90.

BEN-DOR, G. 1991 *Shock Wave Reflection Phenomena.* Springer.

BORIS, J. P., LANDSBERG, A. M., ORAN, E. S. & GARDNER, J. H. 1993 LCPFCT – A flux corrected transport algorithm for solving generalized continuity equations. Laboratory of Computational Physics and Fluid Dynamics, Naval Research Laboratory Report.

CHPOUN, A., PASSEREL, D., LI, H. & BEN-DOR, G. 1995 *J. Fluid Mech.* **301**, 19–35.

HENDERSON, L. F. & LOZZI, A. 1975 *J. Fluid Mech.* **68**, 139–155.

HENDERSON, L. F. & LOZZI, A. 1979 *J. Fluid Mech.* **94**, 541–559.

HORNUNG, H. G. & KYCHAKOFF, G. 1977 *Proc. 11the Intl Symp. Shock Tubes & Waves Seattle, Washington, USA*, pp. 296–302.

HORNUNG, H. G., OERTEL, H. & SANDEMAN, R. J. 1979 *J. Fluid Mech.* **90**, 541–560.

HORNUNG, H. G. & ROBINSON, M. L. 1982 *J. Fluid Mech.* **123**, 155–164.

LANDAU, L. D. & LIFSHITZ, E. M. 1957 *Fluid Mechanics.* Pergamon.

LI, H. 1995 Reconsideration and modification of analytical models of shock and detonation wave reflections. PhD thesis, Dept Mech. Engng, Ben-Gurion University of the Negev.

LIEPMANN, H. W. & ROSHKO, A. 1957 *Elements of Gasdynamics*. John Wiley and Sons.

NEUMANN, J. VON 1963 *Collected Works* (ed. A. H. Taub), vol. 6. Pergamon.

VUILLON, J. 1994 Modelisation et simulation numerique des ecoulement confinés Eulerilus instationaire. PhD thesis, Dept. Milieux hors d'Equilibre, Université de Provence. Marseille.